Research Article

Cancer Immunology Research

High-Affinity GD2-Specific CAR T Cells Induce Fatal Encephalitis in a Preclinical Neuroblastoma Model

Sarah A. Richman[1], Selene Nunez-Cruz[2], Babak Moghimi[1], Lucy Z. Li[2], Zachary T. Gershenson[1], Zissimos Mourelatos[3], David M. Barrett[1], Stephan A. Grupp[1], and Michael C. Milone[2,3]

Abstract

The GD2 ganglioside, which is abundant on the surface of neuroblastoma cells, is targeted by an FDA-approved therapeutic monoclonal antibody and is an attractive tumor-associated antigen for cellular immunotherapy. Chimeric antigen receptor (CAR)–modified T cells can have potent antitumor activity in B-cell malignancies, and trials to harness this cytolytic activity toward GD2 in neuroblastoma are under way. In an effort to enhance the antitumor activity of CAR T cells that target GD2, we generated variant CAR constructs predicted to improve the stability and the affinity of the GD2-binding, 14G2a-based, single-chain variable fragment (scFv) of the CAR and compared their properties *in vivo*. We included the E101K mutation of GD2 scFv (GD2-E101K) that has enhanced antitumor activity against a $GD2^+$ human neuroblastoma xenograft *in vivo*. However, this enhanced antitumor efficacy *in vivo* was concomitantly associated with lethal central nervous system (CNS) toxicity comprised of extensive CAR T-cell infiltration and proliferation within the brain and neuronal destruction. The encephalitis was localized to the cerebellum and basal regions of the brain that display low amounts of GD2. Our results highlight the challenges associated with target antigens that exhibit shared expression on critical normal tissues. Despite the success of GD2-specific antibody therapies in the treatment of neuroblastoma, the fatal neurotoxicity of GD2-specific CAR T-cell therapy observed in our studies suggests that GD2 may be a difficult target antigen for CAR T-cell therapy without additional strategies that can control CAR T-cell function within the CNS. *Cancer Immunol Res; 6(1); 36–46. ©2017 AACR.*

Introduction

GD2 was first identified as a tumor antigen approximately 30 years ago (1), and in 2009 it was number 12 on the National Cancer Institute's list of most promising tumor antigens (2). The target of an FDA-approved monoclonal antibody (dinutuximab), GD2 is a disialoganglioside glycolipid composed of a membrane-buried lipid tail and a small pentasaccharide ectodomain. GD2 is normally present in the developing brains, and to a lesser extent in the adult brain, of humans and rodents, particularly in the cerebellum (3, 4) as well as peripheral nerve cells (5). Its function is not well defined but may be related to cellular migration and/or proliferation (6–9). Due to dysregulation in the stepwise enzymatic processes that build increasingly complex gangliosides from a common precursor, GD2 can be overproduced in certain cancers, most notably the childhood cancer neuroblastoma, melanoma, as well as several types of pediatric sarcomas (1, 10).

Although many different types of cancer cells contain aberrantly high amounts of surface GD2, we focused our efforts here on the pediatric cancer neuroblastoma, the cause of 15% of pediatric cancer deaths. The high-risk category of neuroblastoma has a 5-year overall survival rate of ∼50% despite highly aggressive and toxic multimodal therapy, including GD2 targeted antibody therapy. Thus, more potent $GD2^+$ tumor-targeting therapies are needed, and a natural extension of soluble antibody therapy is CAR T-cell therapy. Chimeric antigen receptor (CAR)–modified T-cell (CART) therapy involves removing a patient's T cells and genetically engineering them *ex vivo* to express a synthetic immunoreceptor consisting of an antigen-binding ectodomain [e.g., single-chain Fv (scFv)] that redirects them to a particular tumor antigen, and signaling domains that trigger T-cell activation and proliferation when antigen is bound. These modified T cells are infused back into the patient where they find and kill antigen-bearing tumor cells. Early-phase I studies of CART therapy targeting GD2 in high-risk neuroblastoma have reported promising results (11, 12), but published studies have thus far been conducted using first-generation CARs (comprised of an antigen-binding domain and the CD247 (CD3ζ) signaling domain only), which are generally less potent than newer generation CARs containing additional costimulatory domains.

[1]Division of Oncology, Department of Pediatrics, Children's Hospital of Philadelphia and Perelman School of Medicine at the University of Pennsylvania, Philadelphia, Pennsylvania. [2]Center for Cellular Immunotherapies, Perelman School of Medicine at the University of Pennsylvania, Philadelphia, Pennsylvania. [3]Department of Pathology and Laboratory Medicine, Perelman School of Medicine at the University of Pennsylvania, Philadelphia, Pennsylvania.

Note: Supplementary data for this article are available at Cancer Immunology Research Online (http://cancerimmunolres.aacrjournals.org/).

Corresponding Author: Michael C. Milone, Perelman School of Medicine of the University of Pennsylvania, 7103 Founders Pavilion, 3400 Spruce Street, Philadelphia, PA 19104. Phone: 215-662-6575; Fax: 215-662-7529; E-mail: milone@mail.med.upenn.edu

doi: 10.1158/2326-6066.CIR-17-0211

The generation of optimized CART therapies is largely empiric. Beyond incorporation of costimulatory domains to enhance T-cell survival and persistence (13, 14), modifications of scFv affinity for the target antigen, as well the ectodomain structure, can influence CAR T-cell function (15, 16). In this study, we evaluated changes to both scFv affinity and linker structure that were expected to improve the function of a previously described GD2-specific CAR construct (17). We observed that changes predicted to produce a more stable and higher affinity scFv markedly improved the *in vivo* and *in vitro* function of a GD2-specific CAR. However, we also observed that these improvements in function were associated with lethal "on-target, off-tumor tissue" toxicity. Together, these results indicate that effective targeting of GD2 by CAR T cell–based therapies may be challenging.

Materials and Methods

CAR constructs

Plasmid DNA encoding the GD2-specific, 14G2a murine antibody-based scFv plasmid was generously provided by Dr. Malcolm Brenner, Baylor College of Medicine, Houston, TX (17). The linker separating the variable domains was changed to $(Gly_4Ser)_4$ (synthesized by Genewiz), and the E101K mutation was introduced into the CDR3 of the V_H domain by gene synthesis (Genewiz). ScFvs were ligated into a lentiviral vector, downstream of an EF1α promoter and in frame with the *CD8A* hinge and transmembrane domains and the cytoplasmic domains of *TNFRSF9* (4-1BB) and *CD247* (CD3ζ) to create the scFv-CD8 hinge-4-1BB-CD3ζ CAR constructs [referred to as GD2, GD2 "extended linker" (XL), and GD2-E101K, respectively]. A negative control FMC63-based anti-CD19-CD8 hinge-4-1BB-CDζ was used in this study, referred to as "CD19 CAR." The m3F8-based CAR was constructed using publicly available variable domain sequence (18). Variable domains were positioned on either side of a $(Gly_4Ser)_4$ linker in both possible orientations (V_H-linker-V_L and V_L-linker-V_H). The scFv portions were synthesized (Genewiz) and ligated into lentivirus to create CD8 hinge/transmembrane-4-1BB-CD3ζ CARs. Only the V_L-linker-V_H orientation resulted in functional CAR.

Isolation, transduction, and expansion of human primary T lymphocytes

Human primary T cells collected from healthy volunteers were obtained from the Human Immunology Core at the University of Pennsylvania. Cells were expanded with anti-CD3/anti-CD28–coated beads and transduced with lentivirus as described previously (19) at a multiplicity of infection of 5–7. T cells were cultured in media without additional cytokines until they had rested down with a cellular volume of approximately 400 fL, ranging from days 9 to 14 depending on the T-cell donor. Upon resting down, beads and media were removed, and the cells were washed in Dulbecco's phosphate-buffered saline (PBS), resuspended in fetal bovine serum (FBS) with 5% dimethylsulfoxide (DMSO) for cryopreservation at −150° C. Rested frozen T cells were thawed and washed with media prior to *in vitro* assays or further preparation for injection into mice. Bulk human T cells were used for *in vitro* experiments. For *in vivo* experiments, purified $CD4^+$ and $CD8^+$ populations were obtained from the core and then mixed at a ratio of 1:1 prior to expansion.

Mouse IgG2a expression and purification

The variable domains of the GD2 and E101K scFvs were cloned into expression vectors pFUSE2ss-CLIg-mK and pFUSEss-CHIg-mG2a (Invivogen, cat no. pfuse2ss-mclk and pfusess-mchg2a) containing the IL2 secretion sequence and respective mouse κ light and IgG2a heavy constant regions. These plasmids were then transiently transfected into FreeStyle 293-F cells (3×10^7) grown in serum-free media (Invitrogen, cat no. R790-07 and Thermo Fisher, cat no. 12338018). Supernatants were collected after 6 days, concentrated, and secreted IgG was purified using a Protein A resin spin column (Thermo Scientific, cat no. 89960) per manufacturer's instructions. Purified antibody was then concentrated and buffer-exchanged for further in staining cells for flow cytometry.

Flow cytometric analysis

PBS-washed pelleted T cells on day 8 of expansion were incubated with biotin-SP-AffiniPure Goat Anti-Mouse IgG $F(ab')_2$ Fragment Specific (Jackson ImmunoResearch Laboratories, Inc., cat no. 115-065-072) primary antibody at approximately 0.075 mg/mL for 15 minutes at room temperature. Cells were then washed three times in 2 mL room temperature PBS, and the pellet was resuspended in R-phycoerythrin-conjugated streptavidin (SA: PE; BD Biosciences, cat no. 349023) at approximately 0.08 μg/mL for 5 minutes at room temperature. For staining of cell lines, trypsinized, PBS-washed tumor line cells were incubated with anti-GD2-PE, clone 14G2a (BioLegend, cat no. 357304), purified anti-GD3 (Abcam, cat. no AB11779), or respective isotype controls at 1:30 dilution for 15 minutes at room temperature. For the anti-GD3 staining, after primary antibody incubation, cells were washed once with 2 mL room temperature PBS and then resuspended in goat anti-mouse AF 647 (Life Technologies, cat no. A-21235) at a 1:60 dilution for 15 minutes at room temperature. Following staining, cells were washed in 2 mL room temperature PBS. For the dissociation analysis, SY5Y cells were washed, pelleted, and incubated with 1 μg antibody on ice for 30 minutes. Cells were then washed three times with 30 volumes each ice-cold buffer. Cells were then resuspended in 50 volumes of room temperature buffer, and at various time points, an aliquot was removed and immediately added to ice-cold buffer and placed on ice. Cells were then washed once with ice-cold buffer, incubated with goat anti-mouse AF647 secondary antibody for 20 minutes on ice, and washed again in ice-cold buffer. After the final wash, cells were fixed in 1% paraformaldehyde and analyzed on an LSR II flow cytometer (BD). Data points were then fitted to a nonlinear curve and using a one-phase exponential decay equation in GraphPad Prism using the model $Y = (Y_0 - \text{background})^*\exp(-k\ ^*X) + \text{background}$.

Cell lines

293T cells were propagated as described previously (13). 293-F cells were purchased from Invitrogen (see above) and propagated in FreeStyle media per manufacturer's instructions (see above). Human neuroblastoma cell lines SY5Y and NB16 were a generous gift of Dr. John Maris, Children's Hospital of Philadelphia, Philadelphia, PA, and 143b osteosarcoma, SK-MEL melanoma, and A431 epidermoid carcinoma cell lines were purchased from ATCC. Tumor cell lines were maintained in DMEM media supplemented with 10% FBS, 10 mmol/L HEPES buffer, 100 U/mL penicillin, and 100 g/mL streptomycin sulfate, with the exception of A431, where RPMI 1640 was substituted for DMEM. Adherent

cells were enzymatically dissociated with trypsin-ETDA 0.25%. The SY5Y-click beetle green (CBG) luciferase line ("SY5Y-CBG") was created by transducing the SY5Y parental line with lentivirus encoding CBG luciferase and green fluorescent protein, separated by a T2A self-cleaving peptide. Following transduction, the cells were expanded and sorted by fluorescence-activated cell sorting (FACS) to obtain a population > 95% GFP positive. The growth and morphology of SY5Y-CBG cells in culture as well as surface GD2 antigen density by flow cytometry were evaluated and observed to be indistinguishable from the parental SY5Y cell line. These cells were used at passages 10 to 12 for all experiments with the above characteristics of morphology, growth kinetics, and GD2 antigen density evaluated prior to all experiments. They were also tested for *Mycoplasma* prior to their first use *in vivo* (Lonza MycoAlert kit #LT07-318).

Chromium release assays

Chromium release assays were performed as described in ref. 20, with 14- to 17-hour effector/target coincubations. Non-transduced T cells, or T cells transduced with an irrelevant CAR (e.g., anti-CD19), were included in all experiments to control for alloreactivity between the T-cell donor and the SY5Y tumor line, which is minimal in our experience (perhaps owing to the generally low baseline expression of MHC molecules in the tumor line; ref. 21).

IFNγ release

Supernatant was removed from overnight coincubations of T cells and targets (at an E:T ratio of 5-10:1). IFNγ concentration present in the supernatants was determined by ELISA (R&D, cat. no. DY295). Each individual experiment was performed in triplicate.

Proliferation assays

The indicated targets were irradiated with 100 Gy and then plated in 24-well plates at a density of 0.5×10^6 target cells per plate. T cells (1×10^6 per well) were then added to the wells, and absolute T-cell count was measured using CountBright absolute counting beads (Life Technologies, cat no. C36950) at days 4, 6, and 8. New media were added and cells were transferred to larger containers depending on rate of T-cell proliferation. The experiment was performed in triplicate.

In vivo xenograft experiments

NOD-SCID-*Il2rg*$^{-/-}$ (NSG) mice were housed in the Xenograft Core Facility at the University of Pennsylvania under pathogen-free conditions, and experimental protocols were approved by the University of Pennsylvania IACUC. Six- to 8-week-old NSG mice were injected with 0.5×10^6 SY5Y-CBG cells in 100 μL PBS via tail vein on day 1 (control groups received 100 μL PBS alone). On day 5, mice were randomly assigned amongst all cages to receive one of four types of CAR T cells: GD2 CAR, GD2-XL CAR, GD2-E101K CAR, or CD19 CAR (negative control for alloreactivity between donor T cells and tumor line), or PBS alone, such that each cage contained a mix of mice receiving different T cells. Mice randomized to receive CAR T cells were injected with 3×10^6 CAR$^+$ human T cells (~5 million total cells total including the subpopulation negative for CAR by flow cytometry) that had been isolated, transduced, and expanded as described above, cryopreserved at −150° C in FBS with 5% DMSO, thawed, washed, counted, assessed for viability, and resuspended in PBS on the day of injection. A test batch of each CAR T cell was evaluated *in vitro* prior to injection into mice to confirm activity. T cells (100 μL) in PBS or PBS alone were injected into each mouse via tail vein. Tumor burden was assessed by measuring *in vivo* bioluminescence of anesthetized mice 4, 11, 18, 24, 31, and 36 days after tumor injection using on an IVIS Spectrum imager running Living Image software (PerkinElmer) following intraperitoneal injection of 2.27 mg (~115 mg/kg) firefly D-luciferin (Caliper Life Sciences). Most mice were sacrificed due to large tumor burden, signs of CNS-related toxicity, or due to the end of the experiment.

Syngeneic mouse experiments

Naïve T cells from 129 × 1/SvJ mice were isolated using EasySep kit (STEMCELL Technologies, cat. no. 19851) and transduced with MSGV retrovirus encoding a CAR construct consisting of the E101K V_L-$(G_4S)_4$-V_H scFv described here linked to the murine *Cd28*-hinge, transmembrane, and intracellular domains and *Cd247* (CD3ζ) (22). The intracellular components were a generous gift of James Kochenderfer (NCI). In a preliminary experiment, five million mouse E101K-CD28-CD3ζ CAR$^+$ T cells were injected via tail vein into syngeneic mice that had been lymphodepleted with 50 mg/kg cyclophosphamide. Mice were then monitored clinically for signs of toxicity compared with mice receiving control CAR T cells.

Tissue processing and histologic analysis

Liver, spleen, brain, heart, and lung were collected from NSG mice at the time of sacrifice, or within 1 day of death for the mice that died without demonstrating appreciable signs of toxicity the day prior. Brains of 129 × 1/SvJ mice were also obtained. Organs were fixed in 10% formalin (Fisher). Formalin-fixed tissue was then paraffin-embedded and processed and stained with H & E at the CHOP Pathology core facility or used for immunohistochemistry.

Immunohistochemistry

Immunohistochemistry of formalin-fixed paraffin-embedded tissue was performed using antibody against human CD8 (Dako cat no. M7103) and human CD4 (Leica cat no. PA0427) at the University of Pennsylvania Perelman School of Medicine Pathology Clinical Service Center. Staining was done on a Leica Bond-IIITM instrument using the Bond Polymer Refine Detection System (Leica Microsystems DS9800). Heat-induced epitope retrieval was done for 20 minutes with ER2 solution (Leica Microsystems AR9640), and antibodies were incubated for 15 minutes, followed by 8-minute post-primary step and 8-minute incubation with polymer HRP, then block endogenous peroxidase for 5 minutes, followed by 10-minute DAB, all at room temperature. Staining slides are washed three times between each step with bond wash buffer or water. Immunohistochemistry on 129 × 1/SvJ brain was performed at the CHOP Pathology core using anti-mouse CD3.

Results

14G2a-based GD2-specific 4-1BB-CD3ζ CAR T cells function *in vitro*, not *in vivo*

We incorporated the original 14G2a-based anti-GD2 scFv into a 4-1BB/CD3ζ second-generation CAR with a CD8α extracellular spacer and transmembrane domain region (Fig. 1A). Primary human T cells were transduced with lentivirus encoding this

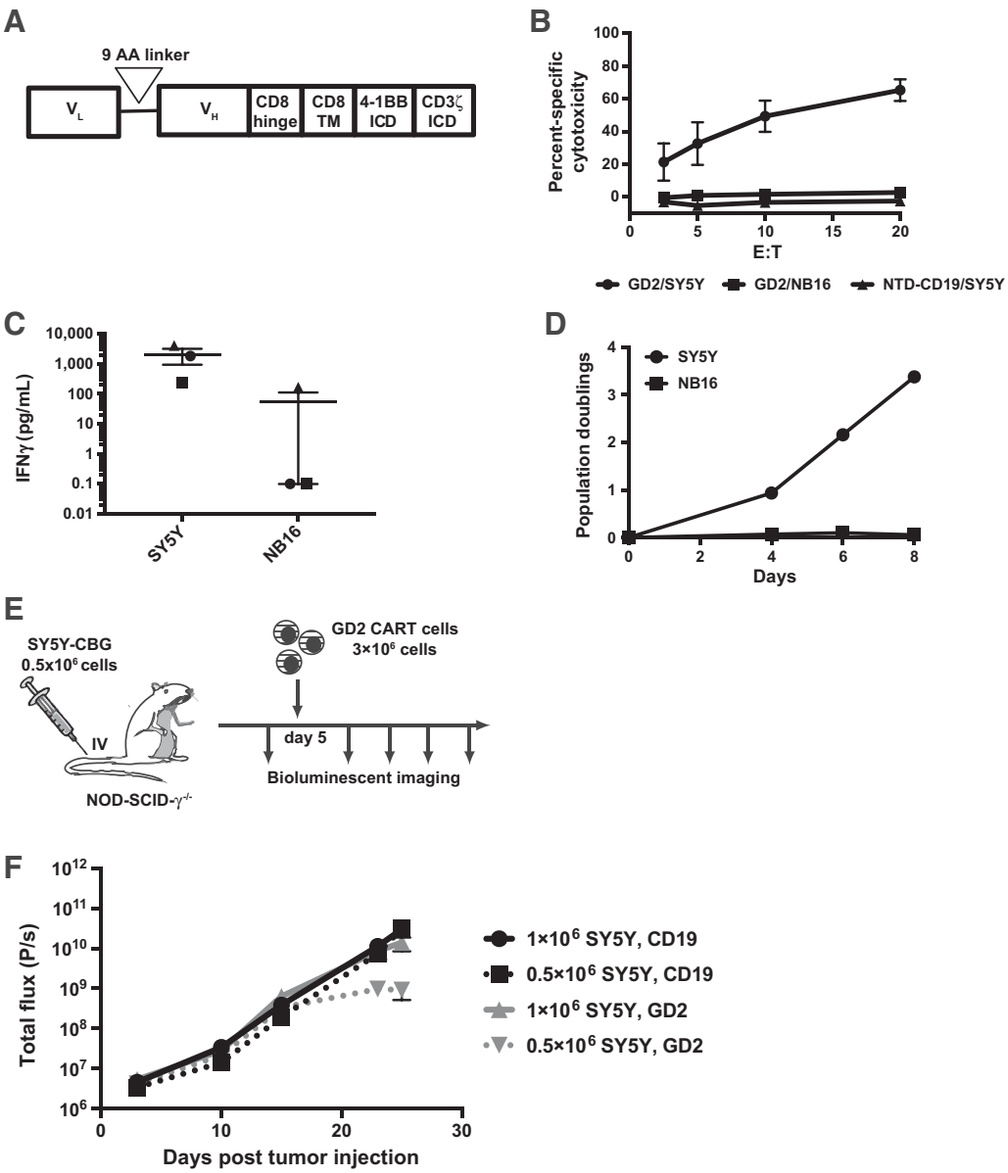

Figure 1.

CAR T cells expressing the original wild-type GD2 CAR display antitumor activity *in vitro* but not *in vivo*. **A,** Schematic of GD2 CAR construct. **B,** Chromium release assay to measure specific cytotoxicity. GD2 CAR T cells were incubated with indicated targets (either $GD2^+$ SY5Y or $GD2^{low}$ NB16), and nontransduced (NTD) T cells, or T cells transduced with an irrelevant CAR (CD19 CAR) were used as a control. Data show mean ± standard error of the mean (SEM) of three separate experiments using three different T-cell donors. **C,** CAR T cells were coincubated with target cells overnight at an E:T ratio of 10:1, and IFNγ in the supernatant was detected by IFNγ ELISA assay. Data include three separate experiments with three different T-cell donors, displayed as points along with the mean ± SEM (■, donor 1; ●, donor 2; ◆, donor 3). **D,** GD2 CAR T cells were incubated with irradiated targets (either SY5Y or NB16), and absolute T-cell count was measured via flow cytometric bead-based counting. The proliferation assay was performed one time in triplicate. **E,** Schematic representation of *in vivo* evaluation of GD2 CAR T cells in NSG mice injected with the SY5Y tumor cells that expressed luciferase. **F,** SY5Y-CBG cells (0.5×10^6 or 1×10^6) were injected via tail vein into NSG mice. On day 5, CD19 or GD2 CAR^+ T cells (3×10^6) were injected via tail vein, five mice per group. Tumor burden was assessed serially by *in vivo* bioluminescence before and after T-cell injection. Data show mean ± standard deviation (SD) from one experiment that was independently confirmed twice using different tumor doses and T-cell injection timing.

GD2 CAR and expanded by culturing with anti-CD3/anti-CD28–coated beads. Following expansion, these CAR T cells were evaluated for *in vitro* and *in vivo* activity against a human neuroblastoma tumor line SY5Y, which expresses high GD2 and, when injected into mice, disseminates and grows rapidly in the liver and to a lesser extent the bone/bone marrow. GD2 CAR T cells exhibited effective cytotoxicity, IFNγ release, and proliferation in response to SY5Y (Fig. 1B, C, and D). We tested these T cells in NSG mice that received a xenograft of our SY5Y-CBG neuroblastoma line cells injected into the tail vein, followed 4 days later by

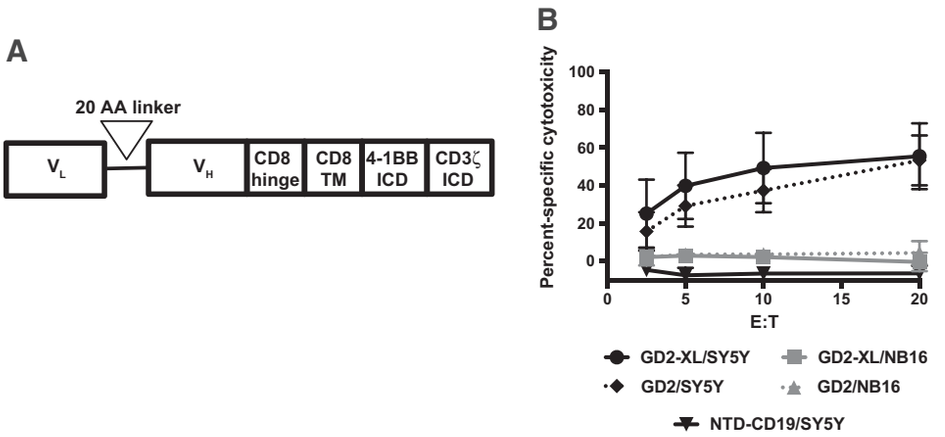

Figure 2.
Lengthening of the linker between variable domains in the GD2 CAR improves activity *in vitro*. **A,** Schematic of the GD2-XL CAR construct. **B,** Chromium release assay to measure specific cytotoxicity, performed as described for Fig. 1. GD2 CAR T cells or GD2-XL CAR T cells were incubated with the indicated targets (either $GD2^{+}$ SY5Y or $GD2^{low}$ NB16), and nontransduced (NTD) T cells or CD19 CAR T cells were used as a negative control. Data show mean ± standard error of the mean (SEM) of three separate experiments using three different T-cell donors.

an injection of GD2 T cells (Fig. 1E and F). The failure of GD2 CAR T cells to completely eradicate tumors *in vivo* in these experiments contradicted a report describing highly effective tumor eradication in a similar experimental condition (23). After comparing growth kinetics of the tumor line used here with that used in the prior report, we attributed the observed differences to the much slower growth kinetics of the tumor cells used in that report compared with the tumor cells used here.

Given the minimal activity of the GD2-CAR T cells when faced with a rapidly growing tumor, we reviewed the structure of the GD2 CAR to identify potential opportunities for enhancing function. The linker between the variable domains of the scFv in our GD2 CAR was short, at 9 amino acids long. Because linker length can affect scFv stability, possibly by constraining intramolecular variable domain pairing, we lengthened the linker to 20 amino acids (Fig. 2A), which in prior studies has provided more optimal scFv conformation (24). GD2 and GD2-XL had comparable CAR surface expression (Supplementary Fig. S1). We then compared the *in vitro* efficacy of the extended linker GD2 CAR (termed GD2-XL) with that of the short-linker construct GD2 and found the extended linker did not improve *in vitro* cytotoxic activity (Fig. 2B).

Enhanced binding affinity to GD2 improved CAR T-cell potency *in vitro*

Although many variables of CAR T-cell construction contribute to potency, we hypothesized that enhancing the affinity of the CAR scFv for GD2 antigen would improve activity. One notable feature of the 14G2a-derived scFv, aside from aspects of its framework region implicated in exhaustive tonic signaling (25), is its relatively low affinity compared with the other antibodies to GD2 in clinical use, such as 3F8 (K_d 77 nmol/L vs. 5 nmol/L of the respective bivalent antibodies; ref. 26). The affinity is also relatively low compared with other CAR scFv:antigen interactions, such as the FMC63 scFv and CD19. The crystal structure of the 14G2a Fab bound to GD2 allowed for the rational design of a higher affinity mutant of the 14G2a antibody, $E101_HK$, which was predicted to allow for improved antigen contact and indeed displayed improved binding in ELISA and flow cytometric assays (27). Consistent with these data, we found the E101K mutation slowed the dissociation kinetics (Supplementary Fig. S2). We thus introduced the affinity-enhancing E101K mutation into the CDR3 of the V_H of our GD2-XL CAR (referred to as GD2-E101K CAR; Fig. 3A).

After establishing the E101K mutation did not appear to significantly alter CAR expression (Supplementary Fig. S1), we evaluated its influence on *in vitro* effector function. GD2-E101K CAR T cells were compared with GD2 and GD2-XL CAR T cells for cytotoxic activity and IFNγ secretion in response to SY5Y target cells. E101K CAR T cells displayed increased *in vitro* cytotoxicity (Fig. 3B). IFNγ secretion was only slightly increased (Fig. 3C). More extensive evaluation of cytotoxic activity across a small panel of cell lines expressing varying levels of GD2 and its precursor GD3, another tumor antigen, demonstrated activity by E101K across a range of GD2 expression including levels not detected by GD2 CAR or GD2-XL CAR. As expected, its activity was independent of the amount of GD3 present (Fig. 3D). The E101K CAR T cells were even capable of some cytotoxic activity and cytokine secretion in response to NB16 (Fig. 3B–D), a neuroblastoma cell line that expresses a low level of GD2 that is barely detectable by flow cytometry. This heightened sensitivity to antigen would be predicted given the enhanced affinity of E101K and is consistent with what has been found previously with other high-affinity scFv-bearing CAR T cells (16, 28).

E101K CAR improved *in vivo* potency and controlled a rapidly proliferating tumor

We next evaluated the ability of E101K CAR T cells to control SY5Y neuroblastoma xenografts in NSG mice as described for Fig. 1. Based upon an analysis of the slope of log-transformed bioluminescence data during the initial 17 days following tumor injection, 5 of the 8 mice receiving the E101K T cells showed significantly slowed tumor growth kinetics compared with the GD-XLT cells (Fig. 4A; Supplementary Fig. S3). The three mice that received E101K CAR T cells and did not demonstrate tumor control displayed absent or very low T-cell engraftment (data not shown). Postmortem evaluation of the livers, where the vast majority of the tumor burden is located, also revealed differences. Grossly, livers from all mice receiving either no T cells, CD19, GD2, or GD2-XL T cells were massively enlarged and nearly completely replaced by innumerable nodules of tumor, while livers from those 5 mice receiving the E101K CAR T cells were virtually indistinguishable from normal liver (Fig. 4B, top row, comparing GD2-XL, E101K, and normal NSG mouse liver). These gross pathologic findings were confirmed by histologic analysis of the livers which demonstrated only very limited areas of normal liver parenchyma with >95% of the liver replaced by tumor in PBS control, GD2, and GD2-XL CAR-treated mice. In contrast, the

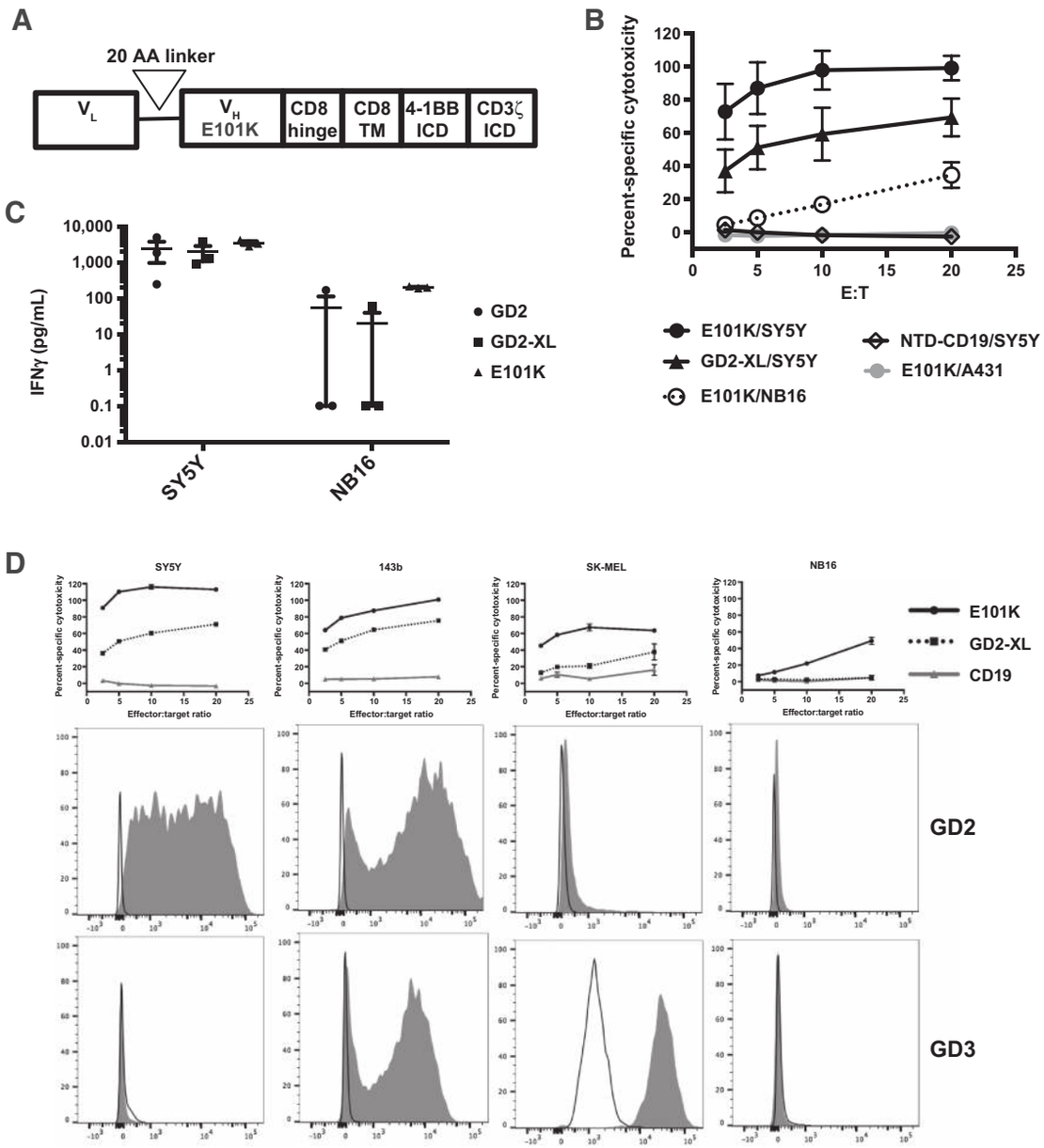

Figure 3.

E101K CAR T cells display enhanced *in vitro* antitumor activity compared with GD2 and GD2-XL CAR. **A**, Schematic of the E101K CAR construct. **B**, *In vitro* cytotoxic activity of GD2, GD2-XL, E101K, and CD19 CAR or NTD T cells was measured in chromium release assay as described for Fig. 1, using the indicated target cells (either the $GD2^{+}$ human neuroblastoma line SY5Y, $GD2^{low}$ human neuroblastoma line NB16, or $GD2^{-}$ epidermoid carcinoma cell line A431.) Data show mean ± standard error of the mean (SEM) of three separate experiments using different three different T-cell donors. **C**, IFNγ secretion was measured as described for Fig. 1 after T cells were coincubated with the indicated target cells. Data include three separate experiments from three different donors, displayed along with mean ± SEM. **D**, Cytotoxic activity of GD2-XL CAR, E101K CAR, or NTD T cells toward different targets with varying surface levels of GD2 and GD3 was evaluated using chromium release assay as described for Fig. 1. The top row depicts percent specific cytotoxicity of CD19 (gray line), GD2-XL (dotted line), and E101K (solid line) CAR T cells from one experiment performed in triplicate. The middle and bottom rows depict flow cytometric histograms of the indicated targets stained with either antibodies to GD2 or to GD3, respectively. Unfilled histograms represent staining with isotype control.

livers of mice treated with E101K CAR T cells revealed mostly normal liver parenchyma with only rare foci of tumor cells comprising less than 1% of the tissue (Fig. 4B). Immunohistochemistry of liver slides stained with antibodies to CD8 and CD4 revealed a predominantly $CD8^{+}$ T-cell infiltration into the livers of mice receiving the GD2-XL CAR T cells. In contrast, at the time of euthanasia livers from E101K mice contained few T cells; their presence was concentrated in the rare small foci of tumor (Fig. 4C). Only the occasional T cell was observed in the livers of mice receiving CD19 CAR T cells, though T cells were

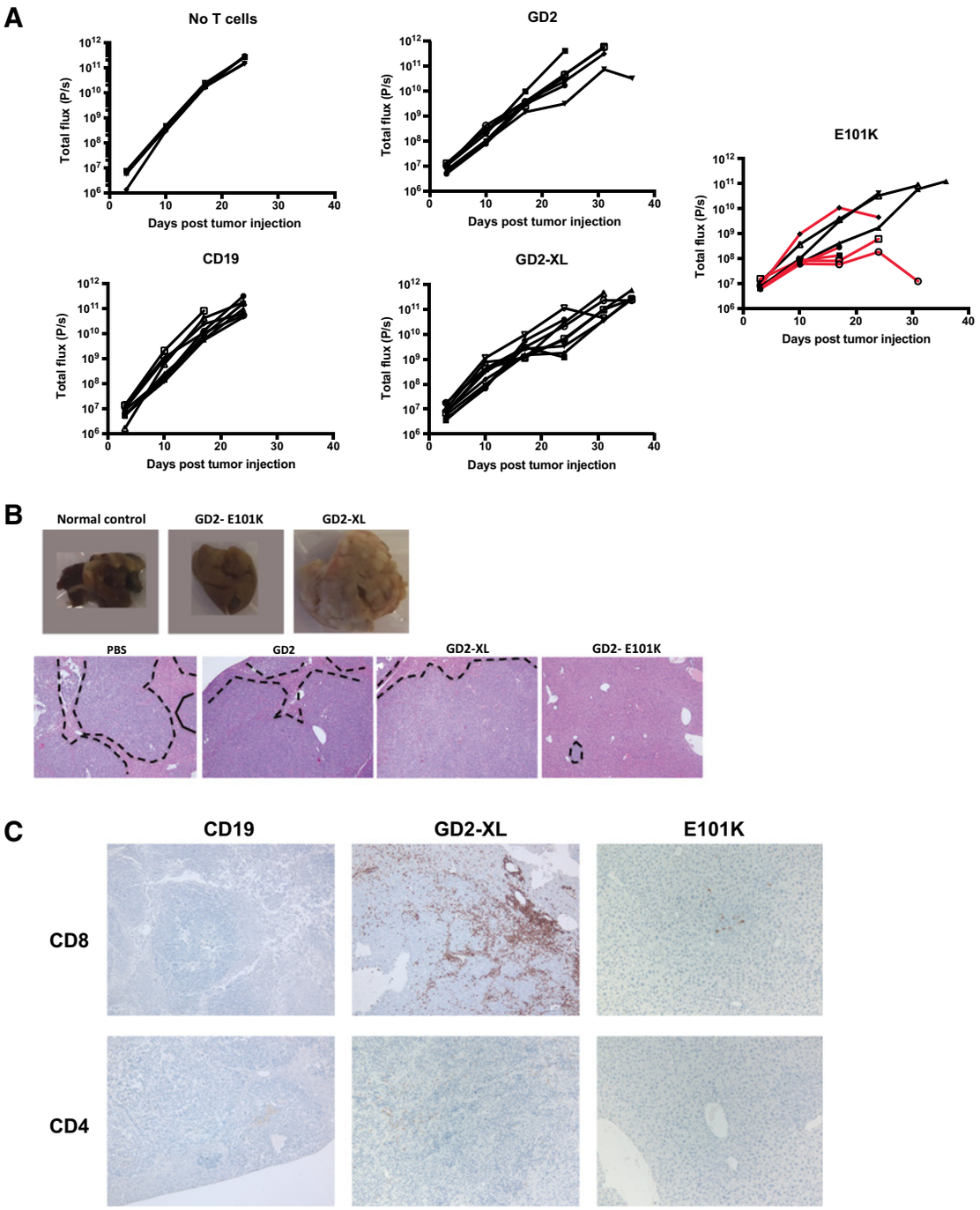

Figure 4.

E101K CAR T cells demonstrate enhanced ability to slow tumor growth as measured by *in vivo* bioluminescence as well as histologic analysis of liver tissue. SY5Y-CBG tumor cells (0.5×10^6) were injected via tail vein into NSG mice. Four days later, T cells (3×10^6 CAR^+) expressing either the GD2 CAR, GD2-XL CAR, E101K CAR, negative control CD19 CAR, or PBS alone were injected via tail vein. Eight mice per group, except the PBS alone group, which contained 5. The data show one experiment. GD2 versus E101K was independently repeated once, and E101K versus NTD or CD19 was independently repeated an additional three times, all with similar results. Tumor burden was evaluated by *in vivo* bioluminescence one day prior to T-cell injection and then at multiple time points thereafter, with the last time point on surviving mice 36 days after tumor injection. **A,** Bioluminescence data, with each curve representing one mouse. Curves of mice receiving E101K CAR T cells that demonstrated CNS toxicity shown in red. **B,** Representative gross liver specimens obtained from mice from the indicated groups (top row). Representative H&E-stained sections of liver from mice in the indicated groups. **C,** Representative anti-human CD8 and CD4 IHC of liver sections from the indicated groups.

present in the spleens in all groups receiving T cells (data not shown).

Tumor control by E101K CAR T cells was associated with severe neurotoxicity

All five of the mice receiving E101K T cells that controlled tumor also displayed signs of neurological toxicity ranging from head tilt and gait disturbance to inactivity, wasting, seizure, and death. The onset of symptoms ranged from 19 to 27 days following T-cell injection with spontaneous death occurring despite low tumor burden. In general, the mice with onset of symptoms at earlier time points tended to be mice with the most robust tumor control. The observed neurological changes were exclusive to mice receiving E101K CAR T cells; mice in other groups did not display these clinical signs. Moreover, the toxicity appeared independent of the presence of tumor, as mice in a control group receiving E101K CAR T cells but no tumor also displayed these clinical changes, though they tended to occur later, with symptom onset ranging from 32 to 36 days following T-cell injection. Similar toxicity was observed in four independent experiments using T cells prepared on separate occasions with different vector stock and T-cell donor. Given the preponderance of neurologic abnormalities, including balance and gait changes observed in the E101K CAR T-cell mice and in light of the reported presence of GD2 in certain regions of normal brain, particularly the cerebellum, we collected brains from all mice to assess for pathology, as well as heart and lung to assess for evidence of more systemic derangements.

Although the gross appearances of the brains were not different, histologic evaluation revealed abnormalities in the E101K group. H&E and IHC staining of sections of brains from mice receiving E101K CAR T cells showed dense cellular infiltrates restricted to certain regions of the brain parenchyma and associated meningeal tissue, particularly the cerebellum, as well as deep gray structures, such as the basal ganglia, thalamus, and midbrain; the cerebral cortex was spared (Figs. 5; Supplementary Fig. S4). CAR T cells were also present in the spinal cord (Supplementary Fig. S5). This infiltrate was composed of large, proliferative cells predominantly $CD8^+$ with numerous mitotic figures present (Fig. 5; Supplementary Figs. S4 and S5). $CD4^+$ T cells were also present. Based on prior studies describing the distribution of GD2 in brains of both rodents and humans, the areas of T-cell infiltration seen in the brains of GD2 E101K-CAR–treated mice correlate with areas of the brain reported to have GD2 expression. No tumor nodules were detected in the brains. Moreover, the T-cell infiltrate was just as pronounced, if not slightly increased, in the mice that did not receive tumor (Fig. 5, bottom row) relative to tumor-bearing mice consistent with this toxicity representing on-target/off-tumor tissue toxicity rather than an *in situ* antitumor effect. A single mouse in the GD2-XL group (which consistently showed robust T-cell engraftment) that received tumor and two of the 5 mice that received GD2-XL T cells but no tumor showed T-cell infiltration into the brain, though to a lesser extent than for E101K. As noted above, only the E101K mice displayed appreciable clinical signs of toxicity. None of the mice receiving GD2 or CD19 CAR T cells were found to have T cells in their brains despite robust engraftment of spleen. None of the mice in this experiment exhibited any of the classic findings of xeno-mediated GVHD (e.g., diarrhea, or skin/coat changes), and the distribution of CNS-infiltrating T cells here was much more focal than that observed in a mouse model of CNS GVHD (29). In a preliminary *in vivo* evaluation, T cells bearing a 4-1BB/CD3ζ CAR based on a separate anti-GD2 antibody, m3F8, in clinical use as monoclonal antibody therapy for neuroblastoma, controlled tumor growth, though the effect was delayed and less robust than observed with the E101K CAR (Supplementary Fig. S6). Neurologic changes were also noted in mice receiving the m3F8 CAR, though these were also delayed and less florid than with E101K. CAR T cells were present in the brain and spinal cord of these mice as well (Supplementary Fig. S5 and data not shown). Similar toxicity findings were also demonstrated in a pilot syngeneic mouse experiment using T cells expanded from splenocytes that were transduced with a retrovirus encoding a fully murine second-generation CAR with a CD28 costimulatory domain (30) and bearing the E101K scFv (E101K-CD28-CD3ζ). Eight to 9 days following T-cell injection, all four mice injected with this CAR demonstrated signs of severe toxicity (seizure, head tilt, impaired mobility). Histologic analysis of the brains from these mice revealed a meningoencephalitis mostly localized to the cerebellum (Supplementary Fig. S7).

Discussion

We have shown here that introducing an affinity-enhancing point mutation into the GD2 CAR significantly improved its potency *in vitro* and *in vivo*, concomitant with the tumor-independent appearance of severe CNS toxicity involving T-cell infiltration into brain regions known to contain GD2. The degree to which a single amino acid substitution increased *in vivo* antitumor activity here was quite striking. Although we might expect CAR T cells bearing a higher affinity antigen receptor to exhibit a lower antigen density threshold (such as that found on normal cerebellum) for activation based on previous findings (16), the dramatic improvement in targeting of the GD2-high tumor line was somewhat surprising. One possible explanation for our findings is that a subset of SY5Y cells may express a level of GD2 just below the threshold antigen density required to trigger killing by the "wild-type" GD2 CAR-engineered T cells. SY5Y exhibits a fairly broad expression pattern spanning greater than 2 logs as measured by flow cytometry (see Fig. 3D). Given the rapidity with which this tumor xenograft proliferates, if even just ∼5% of cells are able to escape killing owing to their subthreshold antigen expression, that subset could conceivably quickly establish a large tumor burden after the GD2-high cells are cleared. Although GD2-XL CAR T cells effectively traffic to the site of and within tumors, as demonstrated by the presence of numerous T cells within the liver tumors (Fig. 4D), we propose that their antitumor response is outpaced by tumor growth. Inversely, the E101K CAR T cells could nearly eradicate the SY5Y cells and are only present in small numbers in the livers of those mice by the time of death. We presume that after killing the vast majority of tumor cells and depleting antigen in the liver, the E101K CAR T cells recirculate away. We cannot exclude the possibility that the improved targeting with E101K CAR T cells may be a result of improved trafficking and retention of T cells within the tumors, which might arise from enhanced activation and secretion of chemotactic signals for further T-cell recruitment. Tracking of GD2 antigen levels on the xenografts over time in mice receiving GD2 CAR T cells may help address the former hypothesis. However, the highly dynamic nature of GD2 levels within tumor cell lines (data not shown) may complicate such analysis. Another possible explanation for the significantly improved efficacy of E101K toward the $GD2^+$ xenograft is that the starting affinity of the GD2 CAR for antigen is suboptimal for any target antigen density (including high density) such that even the cells

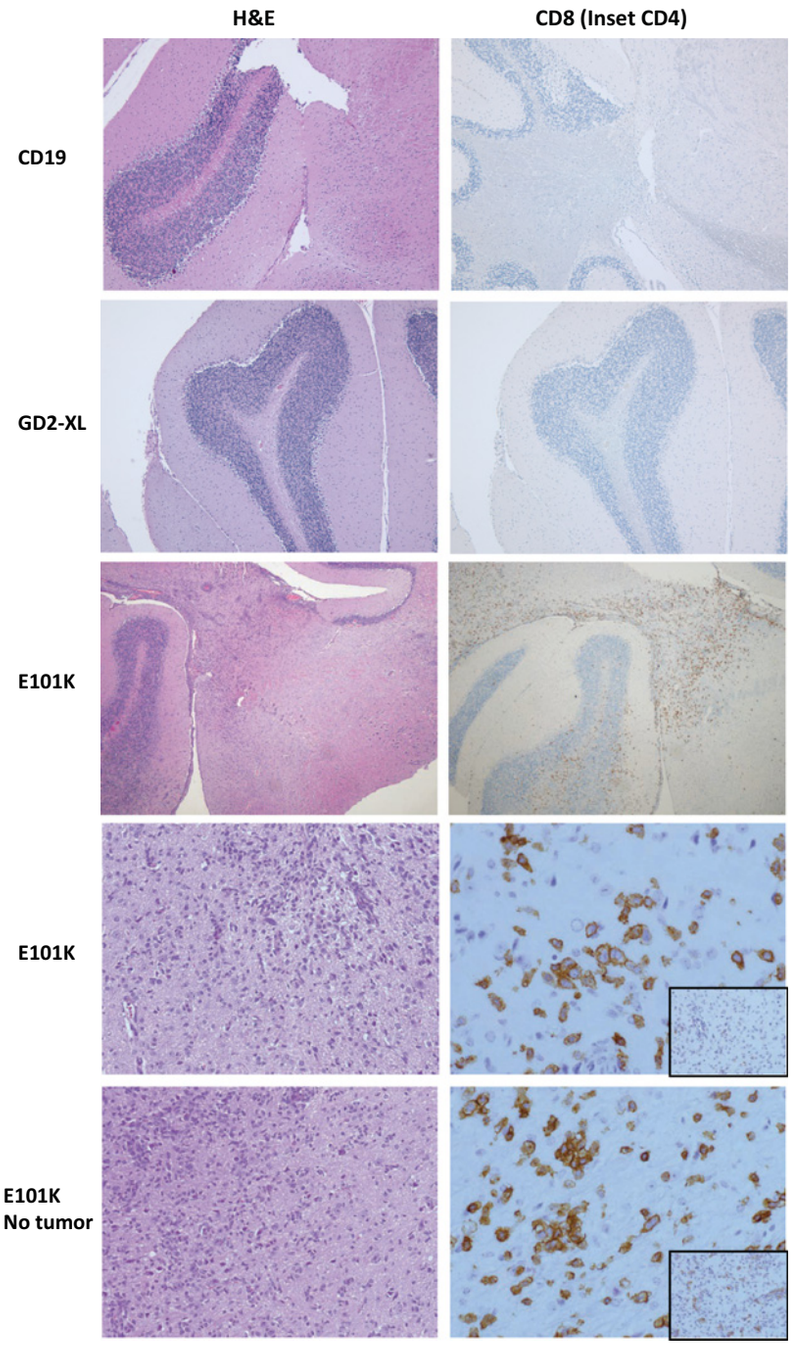

Figure 5.
Serious neurotoxicity is concomitant with tumor control by E101K CAR T cells and associated with CAR T-cell infiltration into brain regions known to contain GD2. Representative H&E (left) and anti-human CD8 and CD4 IHC stained slides (right, CD4 staining is shown in the inset) of brains of mice receiving the indicated CAR T cells. (Top three rows, low power, cerebellum; bottom two rows, H&E 200×, IHC 400×.) Bottom row obtained from the E101K group that did not receive tumor.

with high levels of GD2 are more efficiently killed by the E101K CAR T cells than by the GD2 CAR T cells. Although GD2 antigen density on a particular cell line is challenging to manipulate as the glycolipid is an intermediate product of a complex enzymatic pathway, efforts toward this goal are under way so that we may better understand the role of antigen density *in vivo*.

Given that the GD2 antigen is identical between rodents and humans, a favorable and distinctive feature of this system is that it allows for modeling of on-tumor/off-target toxicity using endogenously expressed antigen. To date, strategies for preclinical modeling of on-target/off-tumor toxicity in the xenograft setting have largely relied on using tumor lines with low levels of antigen to mimic normal tissue. This approach has its limitations given the differences in microenvironment and anatomical niche between tumor and normal tissue and may over- or underestimate toxicity toward normal human tissue. The system described here may thus allow us to determine if there is a GD2-binding affinity range that permits an acceptable therapeutic index, where affinity is high enough that tumor is efficiently controlled *in vivo* yet low enough that normal brain tissue is spared. Other CAR-intrinsic

variables that may be important in discriminating between lower expressing normal tissue and antigen-high tumors, such as the signaling and costimulatory domains as well as the number of surface CAR molecules per cell, can also be evaluated. This model may also be ideally suited to test regulated CAR approaches such as NOT- and AND-gated CARs (31, 32), where an additional tumor-associated antigen can be targeted in order to allow CAR T cells to distinguish normal nervous system tissue from neuroblastoma. Although the impact of CAR-intrinsic variables is the focus of the present study, it is widely recognized that CAR-extrinsic variables (such as T-cell immunophenotype and preinfusion lymphodepletion regimen) also play a major role in the efficacy and safety of these therapies (33). Moreover, the increase in toxicity associated with increased affinity is likely applicable to many different target antigens that are also expressed to some extent on normal tissue, so concepts learned from this model would be expected to be applicable to many different targets where potency is suboptimal but toxicity is also a challenge.

In addition to yielding potential insights into the impact of CAR-intrinsic variables and regulated CAR design on on-target/off-tumor toxicity, the model presented here also represents a novel opportunity to study mechanisms of T-cell trafficking into the CNS, a restricted niche protected by the blood–brain barrier. The critical factors that promote T cells crossing of the blood brain barrier are not completely understood. We hypothesize that a small fraction of CAR T cells initially gain access to the brain parenchyma or nearby perivascular space as part of physiologic cellular immune surveillance of the CNS. Once there, these small number of sentinel CAR T cells encounter antigen in the cerebellum and deep gray matter, and in the case of E101K CAR T cells, such a robust antigen response results in T-cell activation, proliferation (supported by the observed presence of numerous mitotic figures in the affected regions of brain parenchyma), cytotoxicity, and the secretion of chemokines and cytokines attract additional CAR T cells as well as host inflammatory cells such as microglia. Evaluation of cellular brain infiltrates seen in this study by IHC suggests that host cells are also recruited to these infiltrates, and further phenotyping of these cells is under way. A more precise delineation of the chemokines, chemokine receptors, cell adhesion molecules, and their receptors and additional inflammatory cells that are crucial in human T-cell trafficking across the BBB could further our understanding of this important process (in both physiologic and pathologic contexts). As the CNS is not generally a common site of disease in GD2 positive tumors, with the exception of neuroblastoma in relapse, where it occurs in ~20% of patients, and metastatic melanoma, selectively inhibiting the trafficking of T cells into the CNS would theoretically be a translatable approach for targeting GD2 on tumor while reducing the risk of CNS toxicity. As such, in addition to providing a platform to identify potentially targetable factors to protect the CNS in CAR T therapy, it also represents an opportunity for preclinical testing of therapeutics for T-cell–mediated neuroinflammatory disorders such as multiple sclerosis.

Disclosure of Potential Conflicts of Interest

S.A. Grupp reports receiving a commercial research grant from Novartis and is a consultant/advisory board member for the same. M.C. Milone reports receiving a commercial research grant from Novartis. No potential conflicts of interest were disclosed by the other authors.

Authors' Contributions

Conception and design: S.A. Richman, S. Nunez-Cruz, S.A. Grupp, M.C. Milone
Development of methodology: S.A. Richman, B. Moghimi, Z.T. Gershenson, D.M. Barrett, M.C. Milone
Acquisition of data (provided animals, acquired and managed patients, provided facilities, etc.): S.A. Richman, S. Nunez-Cruz, L.Z. Li, Z.T. Gershenson, M.C. Milone
Analysis and interpretation of data (e.g., statistical analysis, biostatistics, computational analysis): S.A. Richman, S. Nunez-Cruz, B. Moghimi, L.Z. Li, Z.T. Gershenson, Z. Mourelatos, D.M. Barrett, S.A. Grupp, M.C. Milone
Writing, review, and/or revision of the manuscript: S.A. Richman, Z.T. Gershenson, D.M. Barrett, S.A. Grupp, M.C. Milone
Administrative, technical, or material support (i.e., reporting or organizing data, constructing databases): S. Nunez-Cruz, M.C. Milone
Study supervision: S. Nunez-Cruz, D.M. Barrett, M.C. Milone

Acknowledgments

This work was supported in part through funding provided by Novartis Pharmaceuticals through a research alliance with the University of Pennsylvania (M.C. Milone) as well as career development awards from the St. Baldrick's Foundation and the NIH (S.A. Richman). S.A. Richman is supported by the St. Baldrick's Foundation Fellowship/Ben's Green Drakkoman Fund and CHOP Cancer Center NIH K12. B. Moghimi is supported by the CHOP Cancer Center Research Training Program NIH T32.

The authors would like to thank John Leferovich and Chune Zhang for their technical assistance, as well as the staff of the Penn Xenograft Core and Small Animal Imaging Facility for their assistance with the in vivo studies. We would also like to thank Daniel Martinez and the staff of theCHOP Pathology core for their expertise and input. We thank Dr. Christopher Hunter for his valuable insight.

The costs of publication of this article were defrayed in part by the payment of page charges. This article must therefore be hereby marked *advertisement* in accordance with 18 U.S.C. Section 1734 solely to indicate this fact.

Received April 21, 2017; revised September 10, 2017; accepted November 14, 2017; published OnlineFirst November 27, 2017.

References

1. Schulz G, Cheresh DA, Varki NM, Yu A, Staffileno LK, Reisfeld RA. Detection of ganglioside GD2 in tumor tissues and sera of neuroblastoma patients. Cancer Res 1984;44:5914–20.
2. Cheever MA, Allison JP, Ferris AS, Finn OJ, Hastings BM, Hecht TT, et al. The prioritization of cancer antigens: a national cancer institute pilot project for the acceleration of translational research. Clin Cancer Res 2009;15:5323–37.
3. Lammie G, Cheung N, Gerald W, Rosenblum M, Cordoncardo C. Ganglioside gd(2) expression in the human nervous-system and in neuroblastomas – an immunohistochemical study. Int J Oncol 1993;3:909–15.
4. Furukawa K, Aixinjueluo W, Kasama T, Ohkawa Y, Yoshihara M, Ohmi Y, et al. Disruption of GM2/GD2 synthase gene resulted in overt expression of 9-O-acetyl GD3 irrespective of Tis21. J Neurochem 2008;105:1057–66.
5. Svennerholm L, Bostrom K, Fredman P, Jungbjer B, Lekman A, Mansson JE, et al. Gangliosides and allied glycosphingolipids in human peripheral nerve and spinal cord. Biochim Biophys Acta 1994;1214:115–23.
6. Dong L, Liu Y, Colberg-Poley AM, Kaucic K, Ladisch S. Induction of GM1a/GD1b synthase triggers complex ganglioside expression and alters neuroblastoma cell behavior; a new tumor cell model of ganglioside function. Glycoconj J 2011;28:137–47.
7. Cazet A, Bobowski M, Rombouts Y, Lefebvre J, Steenackers A, Popa I, et al. The ganglioside G(D2) induces the constitutive activation of c-Met

in MDA-MB-231 breast cancer cells expressing the G(D3) synthase. Glycobiology 2012;22:806–16.
8. Furukawa K, Hamamura K, Aixinjueluo W, Furukawa K. Biosignals modulated by tumor-associated carbohydrate antigens: novel targets for cancer therapy. Ann N Y Acad Sci 2006;1086:185–98.
9. Hettmer S, McCarter R., Ladisch S, Kaucic K.Alterations in neuroblastoma ganglioside synthesis by induction of GD1b synthase by retinoic acid. Br J Cancer 2004;91:389–97.
10. Dobrenkov K, Ostrovnaya I, Gu J, Cheung IY, Cheung NK. Oncotargets GD2 and GD3 are highly expressed in sarcomas of children, adolescents, and young adults. Pediatr Blood Cancer 2016;63:1780–5.
11. Pule MA, Savoldo B, Myers GD, Rossig C, Russell HV, Dotti G, et al. Virus-specific T cells engineered to coexpress tumor-specific receptors: persistence and antitumor activity in individuals with neuroblastoma. Nat Med 2008;14:1264–70.
12. Louis CU, Savoldo B, Dotti G, Pule M, Yvon E, Myers GD, et al. Antitumor activity and long-term fate of chimeric antigen receptor-positive T cells in patients with neuroblastoma. Blood 2011;118:6050–6.
13. Carpenito C, Milone MC, Hassan R, Simonet JC, Lakhal M, Suhoski MM, et al. Control of large, established tumor xenografts with genetically retargeted human T cells containing CD28 and CD137 domains. Proc. Nat.Acad. Sci. U S A 2009;106:3360–5.
14. Hudecek M, Lupo-Stanghellini MT, Kosasih PL, Sommermeyer D, Jensen MC, Rader C, et al. Receptor affinity and extracellular domain modifications affect tumor recognition by ROR1-specific chimeric antigen receptor T cells. Clin Cancer Res 2013;19:3153–64.
15. Hudecek M, Sommermeyer D, Kosasih PL, Silva-Benedict A, Liu L, Rader C, et al. The nonsignaling extracellular spacer domain of chimeric antigen receptors is decisive for in vivo antitumor activity. Cancer Immunol Res 2015;3:125–35.
16. Liu X, Jiang S, Fang C, Yang S, Olalere D, Pequignot EC, et al. Affinity-Tuned ErbB2 or EGFR chimeric antigen receptor T cells exhibit an increased therapeutic index against tumors in mice. Cancer Res 2015;75:3596–607.
17. Rossig C, Bollard CM, Nuchtern JG, Merchant DA, Brenner MK. Targeting of G(D2)-positive tumor cells by human T lymphocytes engineered to express chimeric T-cell receptor genes. Int J Cancer 2001;94:228–36.
18. Ahmed M, Hu J, Cheung NK. Structure based refinement of a humanized monoclonal antibody that targets tumor antigen disialoganglioside GD2. Front Immunol 2014;5:372.
19. Ellebrecht CT, Bhoj VG, Nace A, Choi EJ, Mao X, Cho MJ, et al. Reengineering chimeric antigen receptor T cells for targeted therapy of autoimmune disease. Science 2016;353:179–84.
20. Wang E, Wang LC, Tsai CY, Bhoj V, Gershenson Z, Moon E, et al. Generation of potent T-cell immunotherapy for cancer using DAP12-Based, multichain, chimeric immunoreceptors. Cancer Immunol Res 2015;3:815–26.
21. Reid GS, Shan X, Coughlin CM, Lassoued W, Pawel BR, Wexler LH, et al. Interferon-gamma-dependent infiltration of human T cells into neuroblastoma tumors in vivo. Clin Cancer Res 2009;15:6602–8.
22. Kochenderfer JN, Feldman SA, Zhao Y, Xu H, Black MA, Morgan RA, et al. Construction and preclinical evaluation of an anti-CD19 chimeric antigen receptor. J Immunother 2009;32:689–702.
23. Singh N, Liu X, Hulitt J, Jiang S, June CH, Grupp SA, et al. Nature of tumor control by permanently and transiently modified GD2 chimeric antigen receptor T cells in xenograft models of neuroblastoma. Cancer Immunol Res 2014;2:1059–70.
24. Hudson PJ, Kortt AA. High avidity scFv multimers; diabodies and triabodies. J Immunol Methods 1999;231:177–89.
25. Long AH, Haso WM, Shern JF, Wanhainen KM, Murgai M, Ingaramo M, et al. 4-1BB costimulation ameliorates T cell exhaustion induced by tonic signaling of chimeric antigen receptors. Nat Med 2015;21:581–90.
26. Cheung NK, Guo H, Hu J, Tassev DV, Cheung IY. Humanizing murine IgG3 anti-GD2 antibody m3F8 substantially improves antibody-dependent cell-mediated cytotoxicity while retaining targeting in vivo. Oncoimmunology 2012;1:477–486.
27. Horwacik I, Golik P, Grudnik P, Kolinski M, Zdzalik M, Rokita H, et al. Structural basis of GD2 ganglioside and mimetic peptide recognition by 14G2a antibody. Mol Cell Proteomics 2015;14:2577–90.
28. Chmielewski M, Hombach A, Heuser C, Adams GP, Abken H. T cell activation by antibody-like immunoreceptors: increase in affinity of the single-chain fragment domain above threshold does not increase T cell activation against antigen-positive target cells but decreases selectivity. J Immunol 2004;173:7647–53.
29. Hartrampf S, Dudakov JA, Johnson LK, Smith OM, Tsai J, Singer NV, et al. The central nervous system is a target of acute graft versus host disease in mice. Blood 2013;121:1906–10.
30. Kochenderfer JN, Yu Z, Frasheri D, Restifo NP, Rosenberg SA. Adoptive transfer of syngeneic T cells transduced with a chimeric antigen receptor that recognizes murine CD19 can eradicate lymphoma and normal B cells. Blood 2010;116:3875–86.
31. Roybal KT, Rupp LJ, Morsut L, Walker WJ, McNally KA, Park JS, et al. Precision tumor recognition by T cells with combinatorial antigen-sensing circuits. Cell 2016;164:770–9.
32. Fedorov VD, Themeli M, Sadelain M. PD-1- and CTLA-4-based inhibitory chimeric antigen receptors (iCARs) divert off-target immunotherapy responses. Sci Transl Med 2013;5:215ra172.
33. Turtle CJ, Hanafi LA, Berger C, Hudecek M, Pender B, Robinson E, et al. Immunotherapy of non-Hodgkin's lymphoma with a defined ratio of CD8+ and CD4+ CD19-specific chimeric antigen receptor-modified T cells. Sci Transl Med 2016;8:355ra116.